

# Bayesian Compressive Sensing Failure Detection in Planar Phased Antenna Arrays

M. Salucci, A. Gelmini, G. Oliveri, and A. Massa

## Abstract

The diagnosis of planar phased antenna arrays is dealt with in this work. The retrieval of the faulty radiators in the antenna under test (*AUT*) is formulated within the compressive sensing (*CS*) framework and it is efficiently and effectively solved through a customized Bayesian *CS* (*BCS*) solver. Robust and reliable reconstructions of the *AUT* status are yielded by means of the proposed diagnosis tool also in presence of significant amounts of noise on processed far-field data. Some numerical experiments are presented to assess the *BCS*-based method when dealing with different operative conditions as well as considering a variation of the array size and failure rate.

# Contents

<b>1</b>	<b>Numerical Validation</b>	<b>2</b>
1.1	Taylor Array, $N = 716$ , Isotropic Sources . . . . .	2
1.2	Taylor Array, $N = 1264$ , Isotropic Sources . . . . .	11
1.3	Taylor Array, $N = 1976$ , Isotropic Sources . . . . .	20
1.4	Taylor Array, Analysis vs. Array Size ( $N$ ) . . . . .	29

ELEDIA Research Center

# 1 Numerical Validation

## 1.1 Taylor Array, $N = 716$ , Isotropic Sources

### Parameters

- Gold Array
  - Total number of elements:  $N = 716$ ;
  - Type of elements: isotropic/ideal <sup>1</sup>;
  - Spacing along  $x$  and  $y$ :  $d_x = d_y = 0.5 [\lambda]$ ;
  - Excitation tapering: Taylor;
    - \* Radius:  $R = 7.5 [\lambda]$ ;
    - \* Transition index:  $t = 3$ ;
    - \* Peak sidelobe level:  $PSL = 25$  [dB];

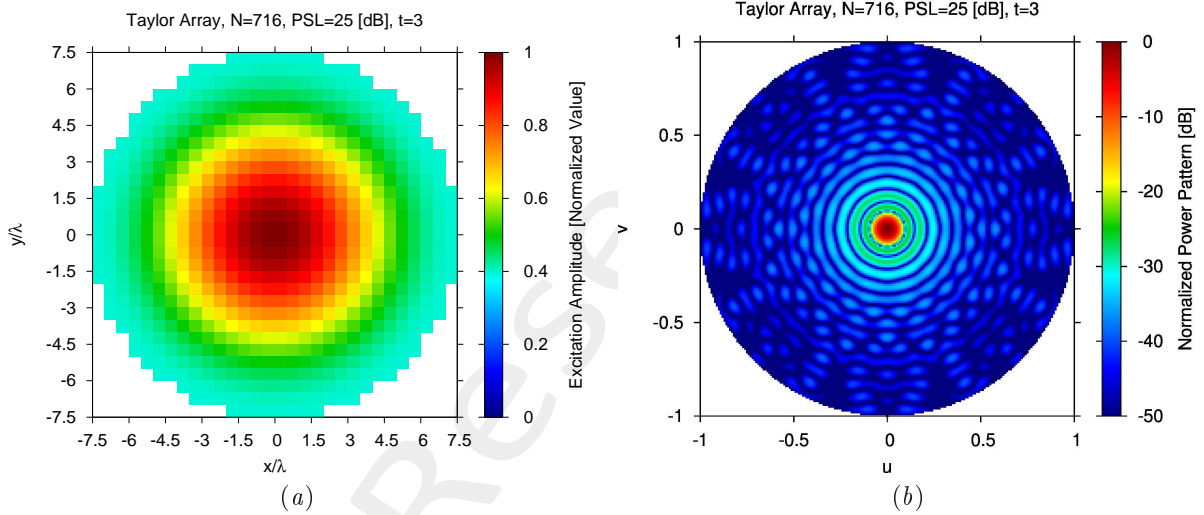


Figure 1: (a) Array excitations and (b) normalized power pattern of the expected array (gold antenna).

- Failed Array
  - Failure factor:  $\kappa = 0$  (total failures);
  - Failure rate: see table below;

$N_f$	$\Phi = \frac{N_f}{N}$
7	1%
14	2%
29	4%
57	8%
115	16%

Table 1: Number of failures ( $N_f$ ) and corresponding failure rate ( $\Phi = \frac{N_f}{N}$ ).

<sup>1</sup>In order to model *isotropic* radiators, let us assume that the embedded elements patterns are equal to  $F_\theta^{(n)}(u, v) = 1$  and  $F_\varphi^{(n)}(u, v) = 0$ , for  $n = 1, \dots, N$ .

- Measurement set-up
  - Type of sampling: uniform sampling in the  $(u, v)$  plane;
  - Number of points in the visible range:  $K = 317$ ;
  - Ratio between measurements and number of elements:  $\nu = \frac{K}{N} \simeq 1.0$  ( $\nu^{(opt)}$ );
- *BCS* solver
  - Noise variance:  $\eta = 5 \times 10^{-1}$  ( $\eta^{(opt)}$ );
  - Tolerance factor:  $\iota = 10^{-8}$ ;
- Signal-to-Noise-Ratio:  $SNR = \{10; 20; \dots; 100\}$ .



## Results

$\Phi = \frac{N_f}{N} = 1\%$  ( $N_f = 7$ ) - Best and Worst *BCS* Reconstructions

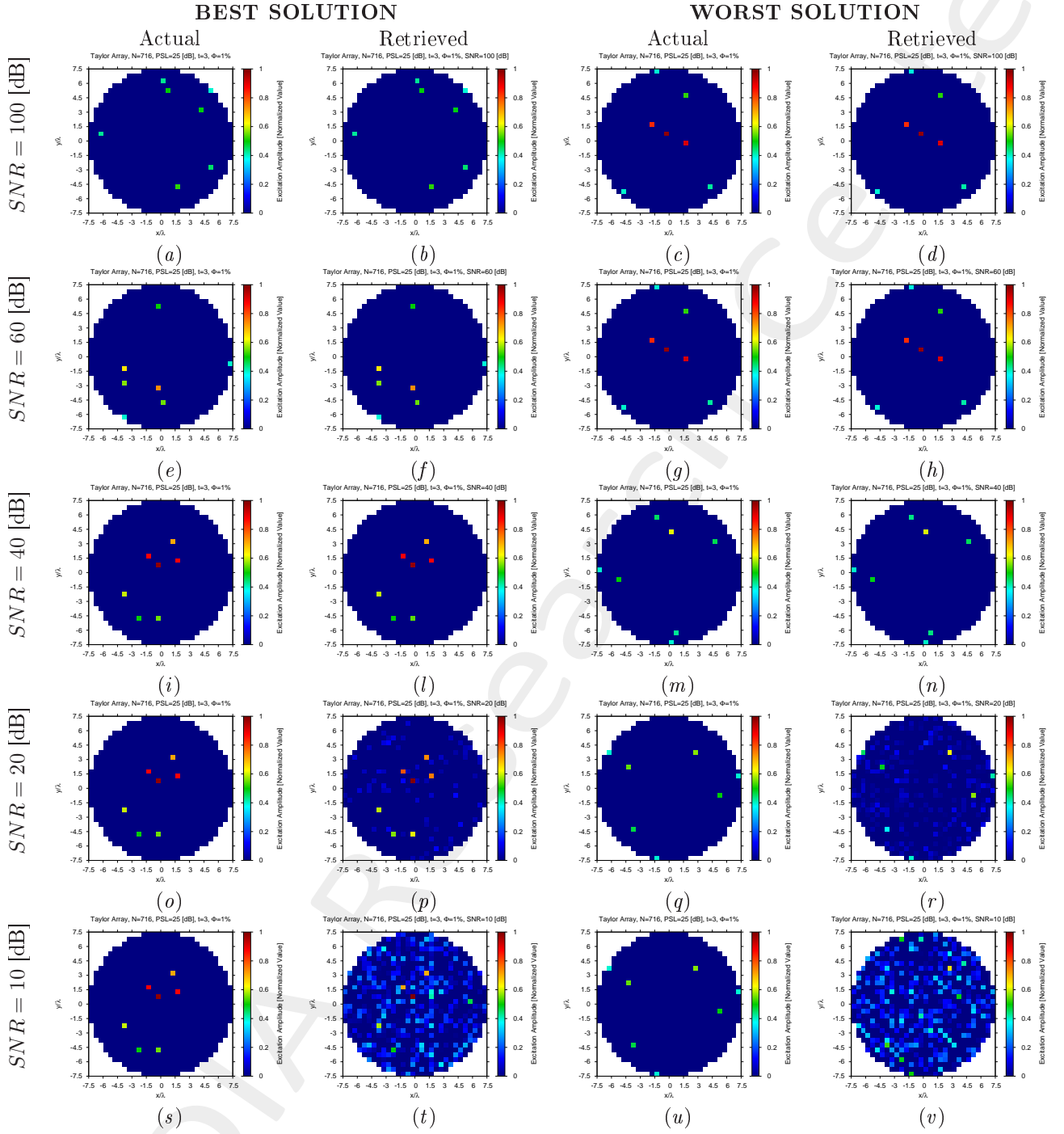


Figure 2: Taylor Array ( $N = 716$ ,  $PSL = 25$  [dB],  $t = 3$ ,  $\Phi = 1\%$ ) - Best and worst reconstructions by *BCS* under several *SNR* values.

$\Phi = \frac{N_f}{N} = 2\%$  ( $N_f = 14$ ) - Best and Worst *BCS* Reconstructions

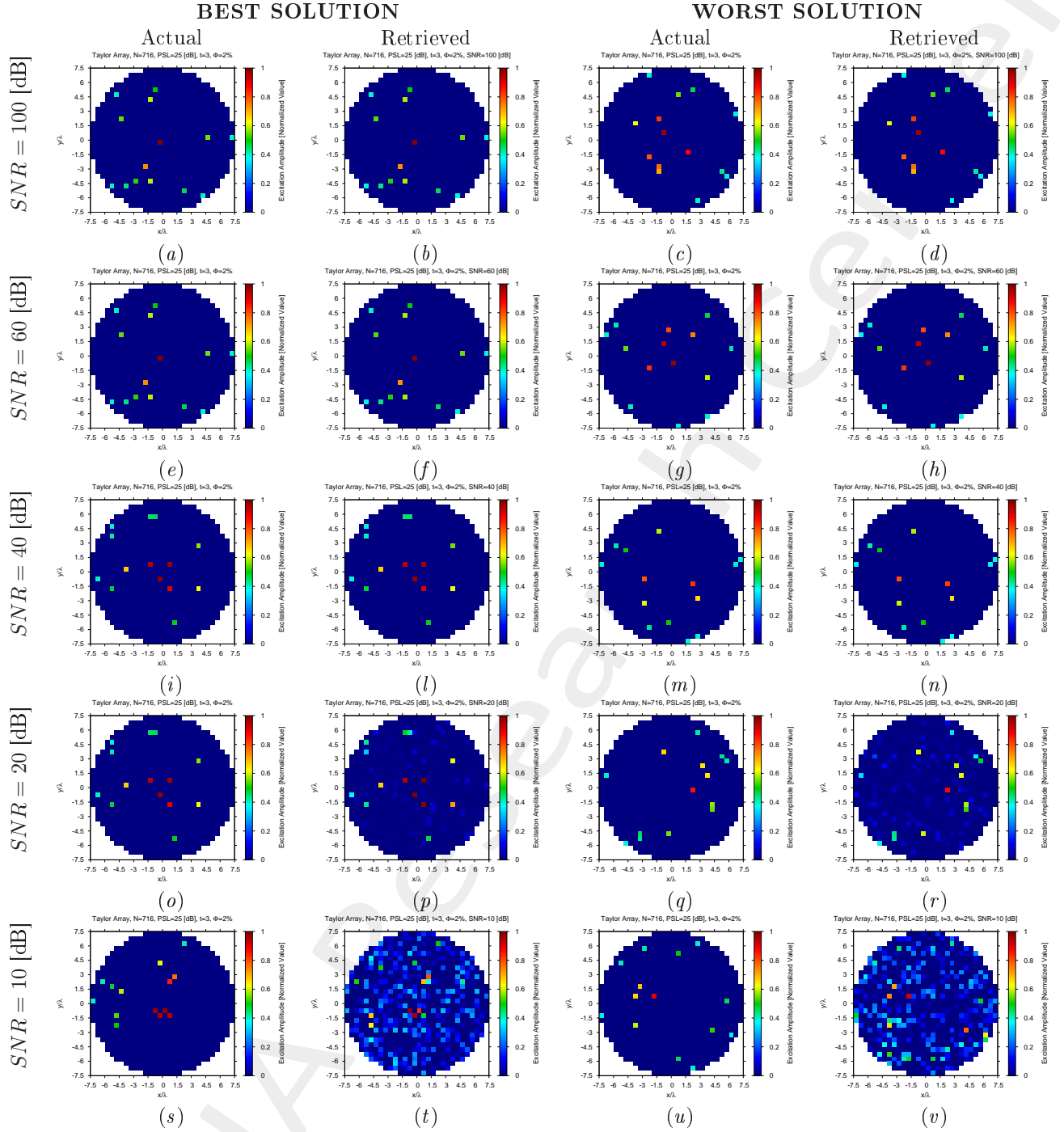


Figure 3: Taylor Array ( $N = 716$ ,  $PSL = 25$  [dB],  $t = 3$ ,  $\Phi = 2\%$ ) - Best and worst reconstructions by *BCS* under several *SNR* values.

$\Phi = \frac{N_f}{N} = 4\%$  ( $N_f = 29$ ) - Best and Worst *BCS* Reconstructions

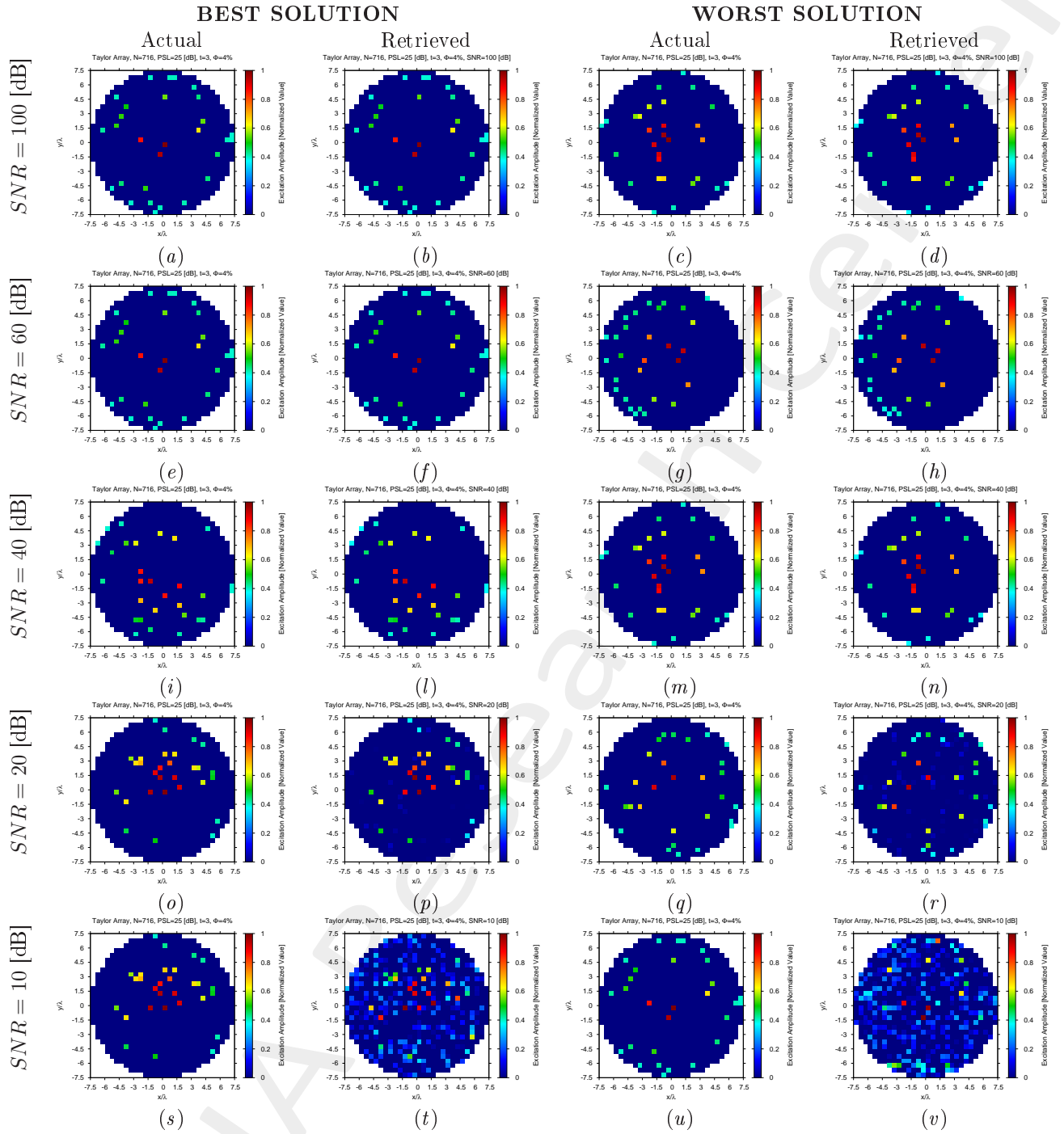


Figure 4: Taylor Array ( $N = 716$ ,  $PSL = 25$  [dB],  $t = 3$ ,  $\Phi = 4\%$ ) - Best and worst reconstructions by *BCS* under several *SNR* values.

$\Phi = \frac{N_f}{N} = 8\%$  ( $N_f = 57$ ) - Best and Worst *BCS* Reconstructions

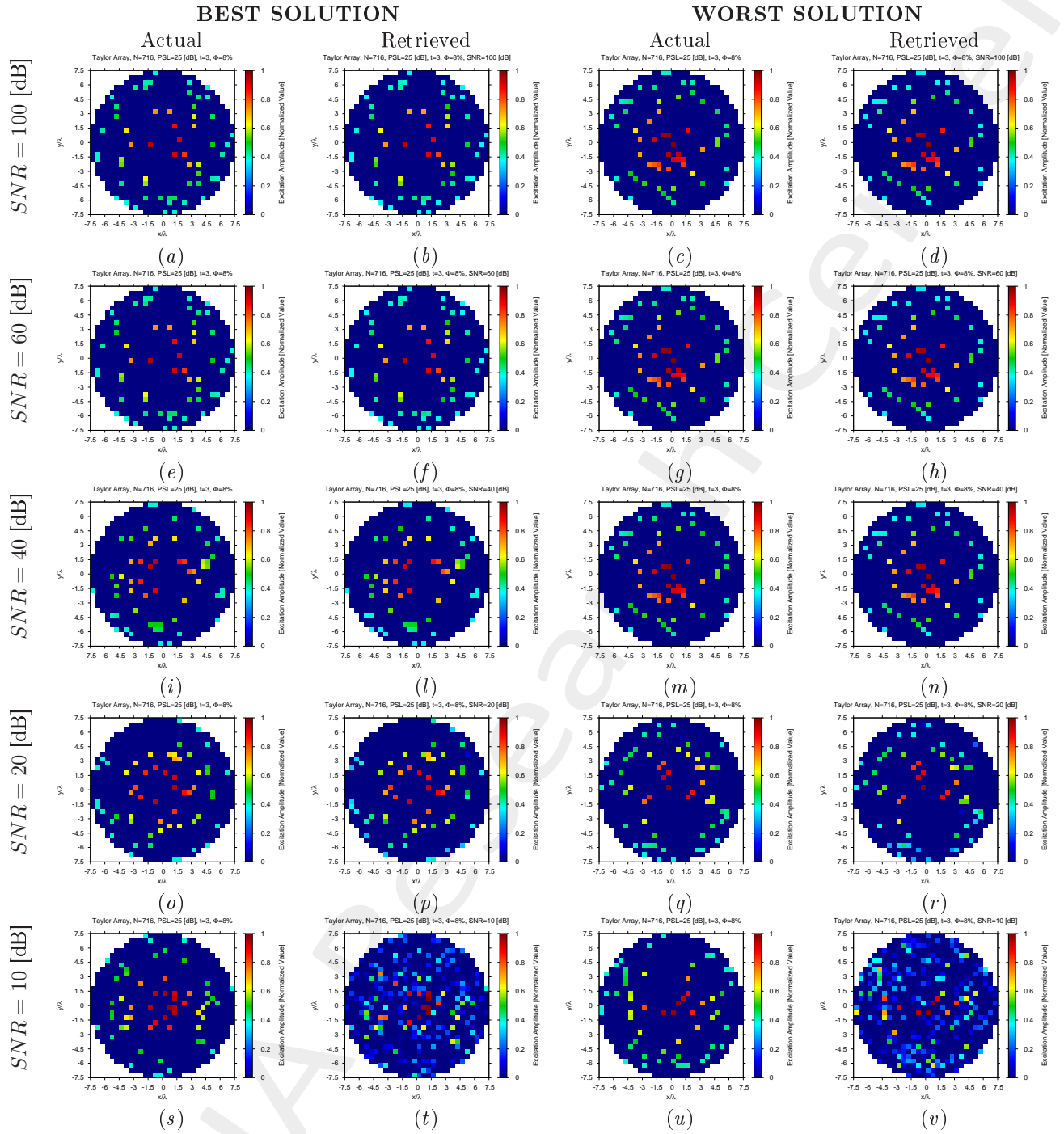


Figure 5: Taylor Array ( $N = 716$ ,  $PSL = 25$  [dB],  $t = 3$ ,  $\Phi = 8\%$ ) - Best and worst reconstructions by *BCS* under several *SNR* values.



## Diagnosis Error and Confidence Level

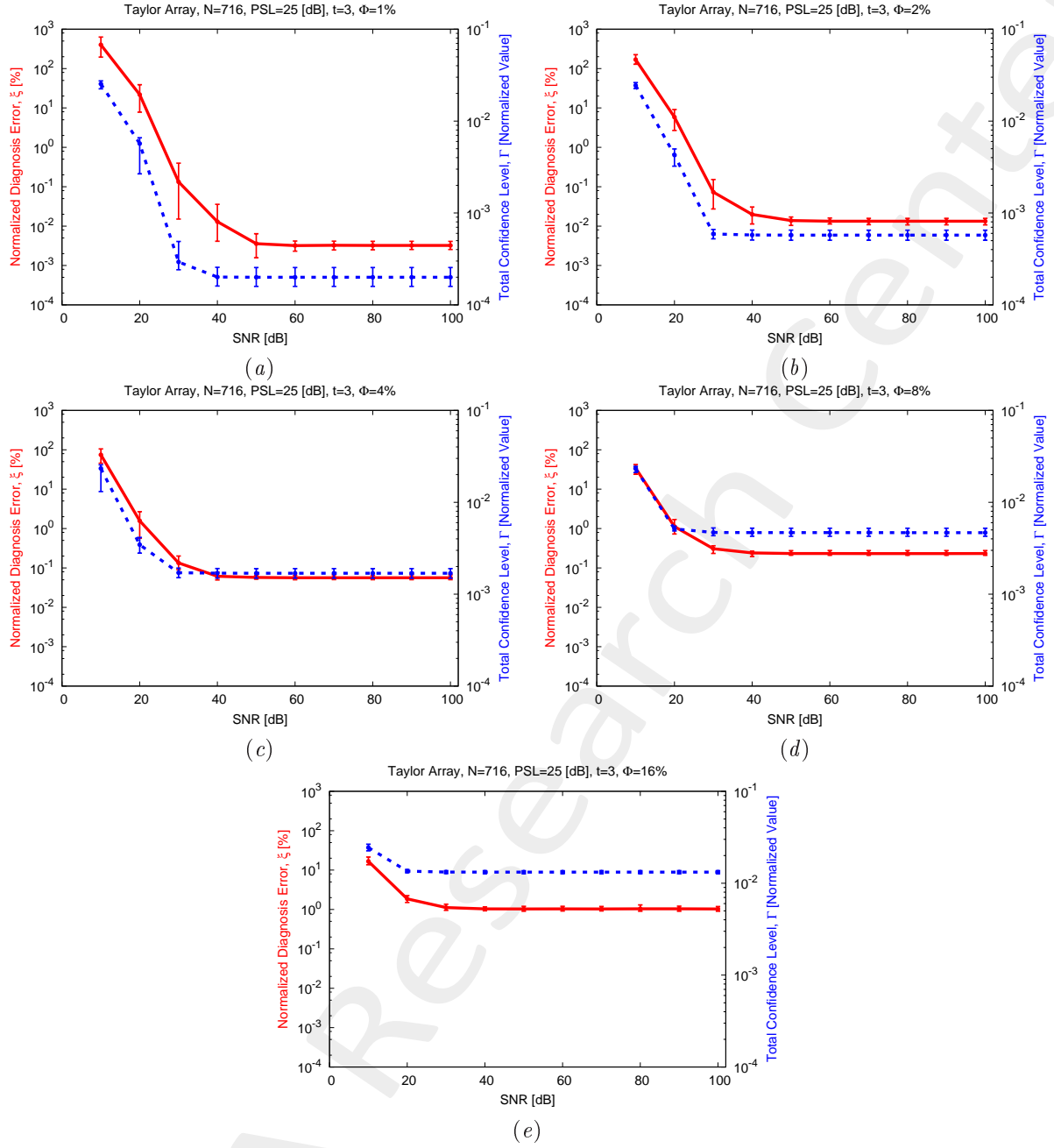


Figure 7: Taylor Array ( $N = 716$ ,  $PSL = 25$  [dB],  $t = 3$ ) - Behavior of the average, minimum and maximum diagnosis error ( $\xi$ ) and total confidence level ( $\Gamma$ ) versus the  $SNR$ , for (a)  $\Phi = 1\%$ , (b)  $\Phi = 2\%$ , (c)  $\Phi = 4\%$ , (d)  $\Phi = 8\%$ , and (e)  $\Phi = 16\%$ .

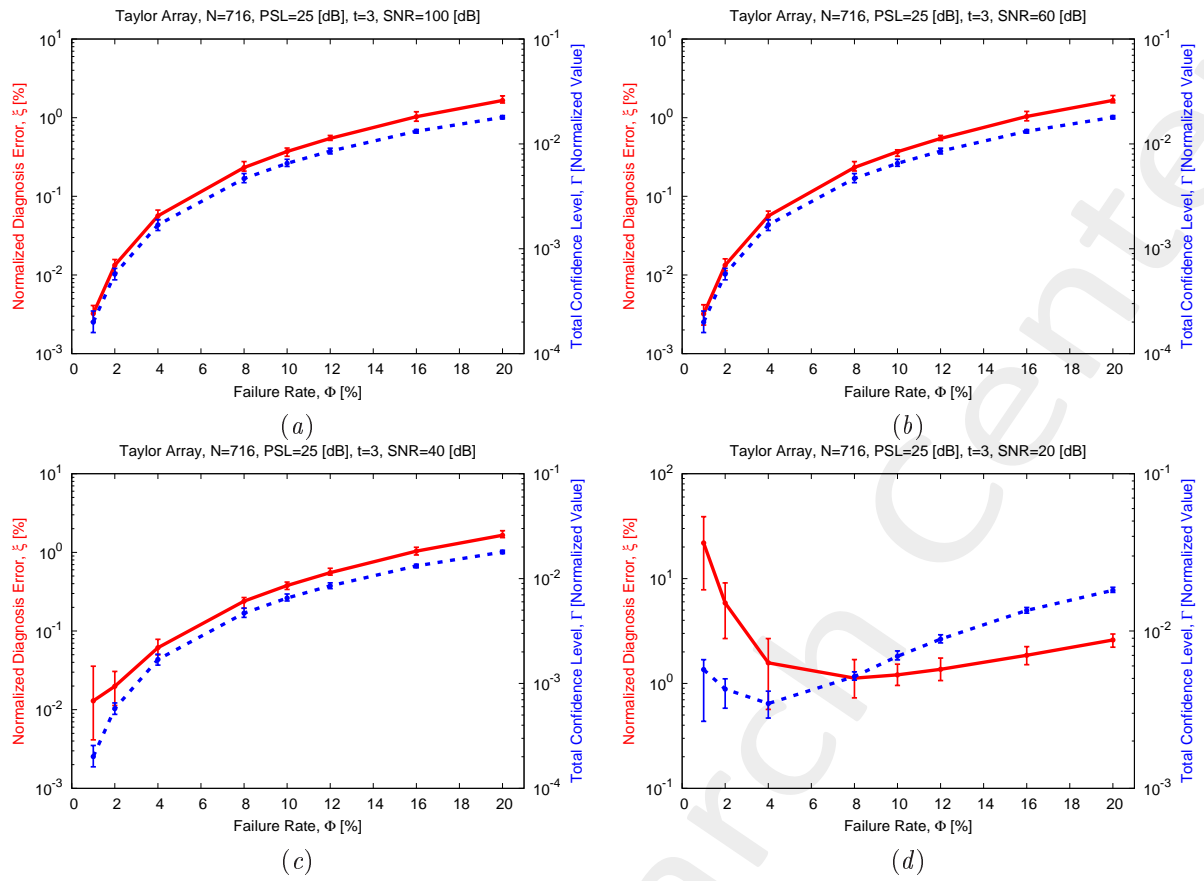


Figure 8: Taylor Array ( $N = 716$ ,  $PSL = 25$  [dB],  $t = 3$ ) - Behavior of the average, minimum and maximum diagnosis error ( $\xi$ ) and total confidence level ( $\Gamma$ ) versus the failure rate ( $\Phi$ ), for (a)  $SNR = 100$  [dB], (b)  $SNR = 60$  [dB], (c)  $SNR = 40$  [dB], and (d)  $SNR = 20$  [dB].

## 1.2 Taylor Array, $N = 1264$ , Isotropic Sources

### Parameters

- Gold Array
  - Total number of elements:  $N = 1264$ ;
  - Type of elements: isotropic/ideal <sup>2</sup>;
  - Spacing along  $x$  and  $y$ :  $d_x = d_y = 0.5 [\lambda]$ ;
  - Excitation tapering: Taylor;
    - \* Radius:  $R = 9.75 [\lambda]$ ;
    - \* Transition index:  $t = 3$ ;
    - \* Peak sidelobe level:  $PSL = 25 [\text{dB}]$

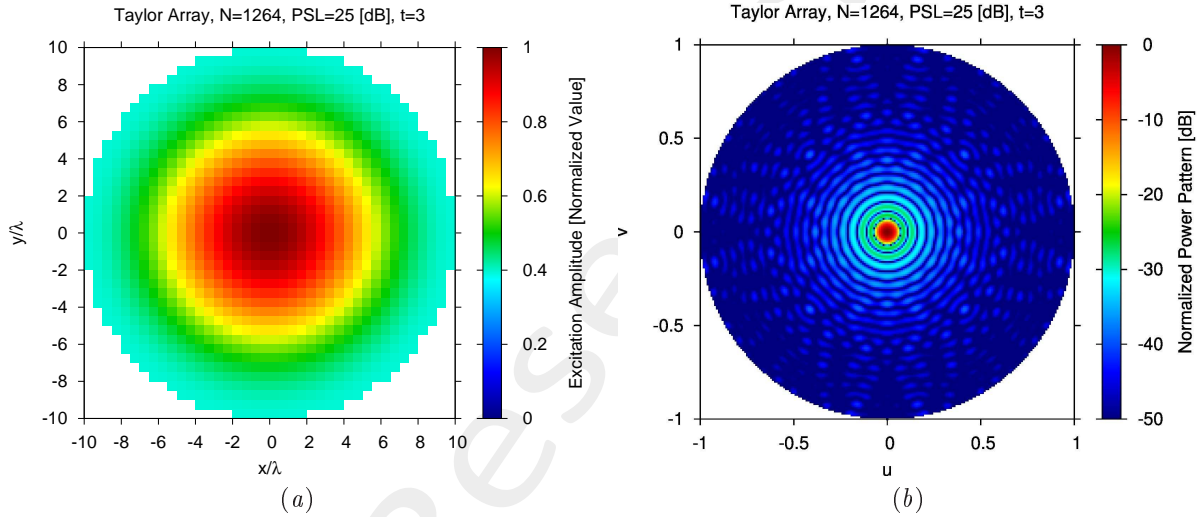


Figure 9: (a) Array excitations and (b) normalized power pattern of the expected array (gold antenna).

- Failed Array
  - Failure factor:  $\kappa = 0$ ;
  - Failure rate: see table below;

$N_f$	$\Phi = \frac{N_f}{N}$
13	1%
25	2%
51	4%
101	8%
202	16%

Table 2: Number of failures ( $N_f$ ) and corresponding failure rate ( $\Phi = \frac{N_f}{N}$ ).

<sup>2</sup>In order to model *isotropic* radiators, let us assume that the embedded elements patterns are equal to  $F_\theta^{(n)}(u, v) = 1$  and  $F_\varphi^{(n)}(u, v) = 0$ , for  $n = 1, \dots, N$ .



- Measurement set-up
  - Type of sampling: uniform sampling in the  $(u, v)$  plane;
  - Number of points in the visible range:  $K = 1257$ ;
  - Ratio between measurements and number of elements:  $\nu = \frac{K}{N} \simeq 1.0$  ( $\nu^{(opt)}$ );
- *BCS* solver
  - Noise variance:  $\eta = 5 \times 10^{-1}$  ( $\eta^{(opt)}$ );
  - Tolerance factor:  $\iota = 10^{-8}$ ;
- Signal-to-Noise-Ratio:  $SNR = \{10; 20; \dots; 100\}$ .

## Results

$\Phi = \frac{N_f}{N} = 1\%$  ( $N_f = 13$ ) - Best and Worst *BCS* Reconstructions

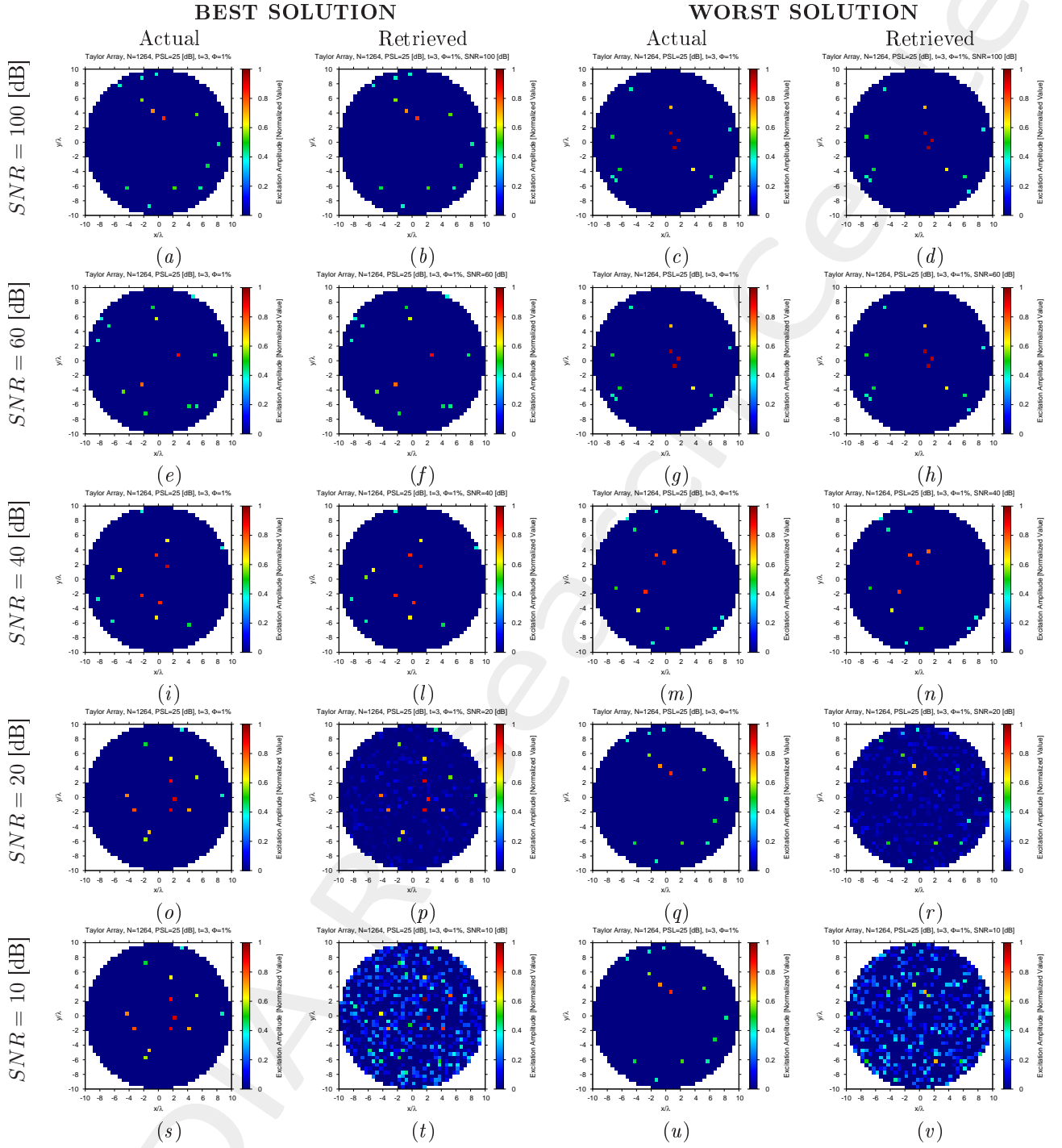


Figure 10: Taylor Array ( $N = 1264$ ,  $PSL = 25$  [dB],  $t = 3$ ,  $\Phi = 1\%$ ) - Best and worst reconstructions by *BCS* under several *SNR* values.

$\Phi = \frac{N_f}{N} = 2\%$  ( $N_f = 25$ ) - Best and Worst *BCS* Reconstructions

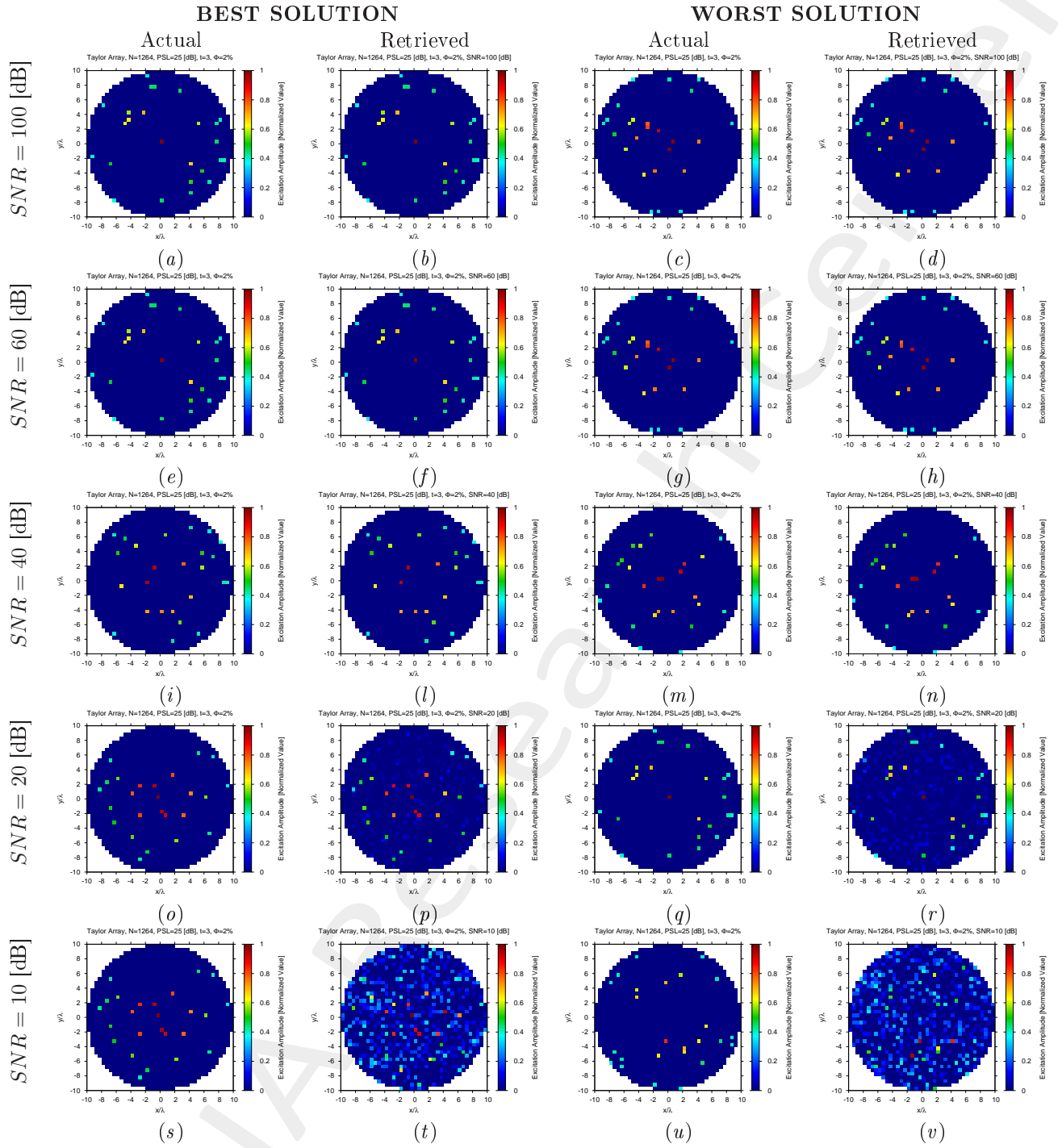


Figure 11: Taylor Array ( $N = 1264$ ,  $PSL = 25$  [dB],  $t = 3$ ,  $\Phi = 2\%$ ) - Best and worst reconstructions by *BCS* under several *SNR* values.

$\Phi = \frac{N_f}{N} = 4\%$  ( $N_f = 51$ ) - Best and Worst *BCS* Reconstructions

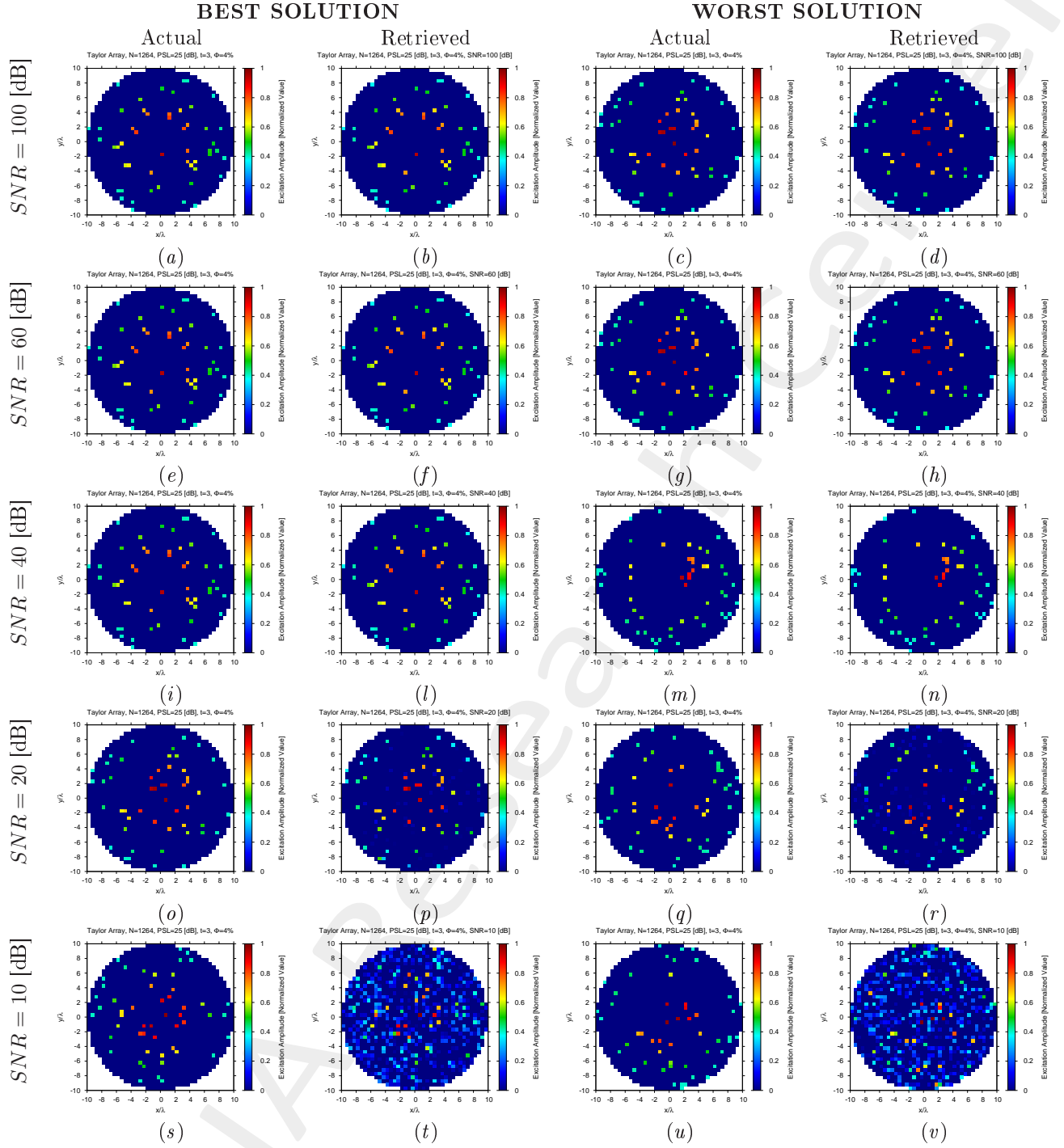


Figure 12: Taylor Array ( $N = 1264$ ,  $PSL = 25$  [dB],  $t = 3$ ,  $\Phi = 4\%$ ) - Best and worst reconstructions by *BCS* under several *SNR* values.

$\Phi = \frac{N_f}{N} = 8\%$  ( $N_f = 101$ ) - Best and Worst  $BCS$  Reconstructions

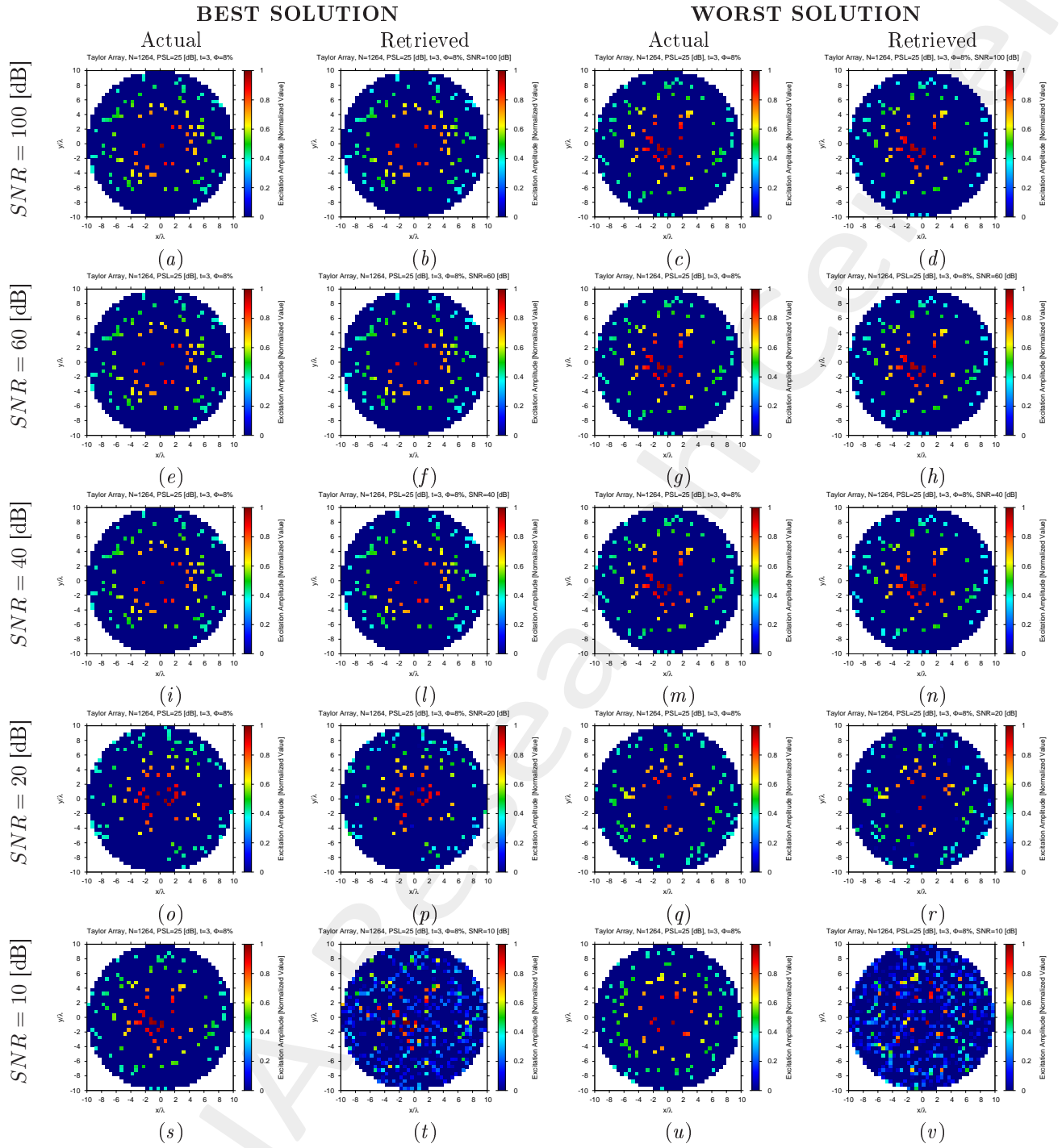


Figure 13: Taylor Array ( $N = 1264$ ,  $PSL = 25$  [dB],  $t = 3$ ,  $\Phi = 8\%$ ) - Best and worst reconstructions by  $BCS$  under several  $SNR$  values.

$\Phi = \frac{N_f}{N} = 16\%$  ( $N_f = 202$ ) - Best and Worst *BCS* Reconstructions

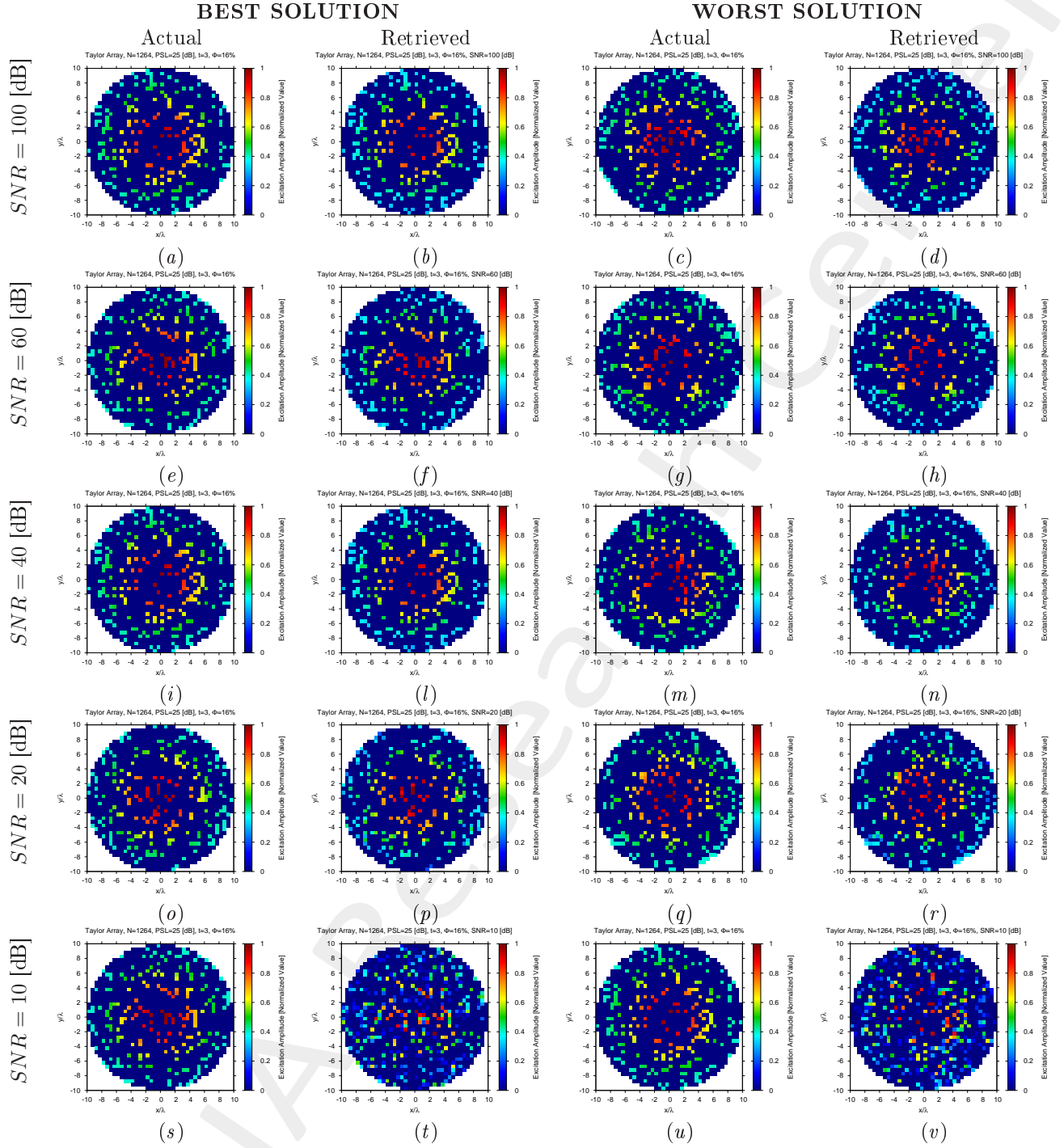


Figure 14: Taylor Array ( $N = 1264$ ,  $PSL = 25$  [dB],  $t = 3$ ,  $\Phi = 16\%$ ) - Best and worst reconstructions by *BCS* under several *SNR* values.

## Diagnosis Error and Confidence Level

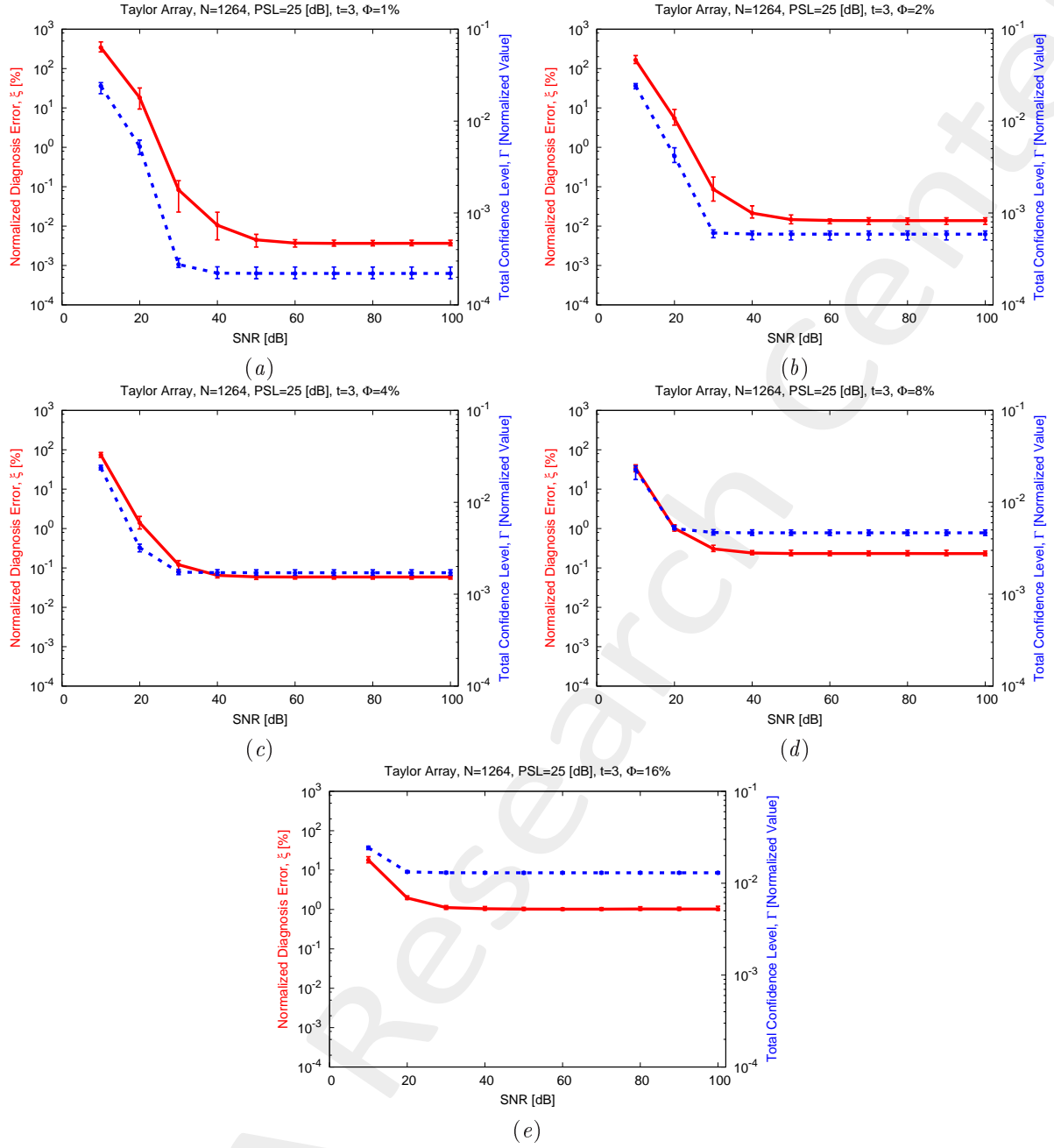


Figure 15: Taylor Array ( $N = 1264$ ,  $PSL = 25$  [dB],  $t = 3$ ) - Behavior of the average, minimum and maximum diagnosis error ( $\xi$ ) and total confidence level ( $\Gamma$ ) versus the  $SNR$ , for (a)  $\Phi = 1\%$ , (b)  $\Phi = 2\%$ , (c)  $\Phi = 4\%$ , (d)  $\Phi = 8\%$ , and (e)  $\Phi = 16\%$ .

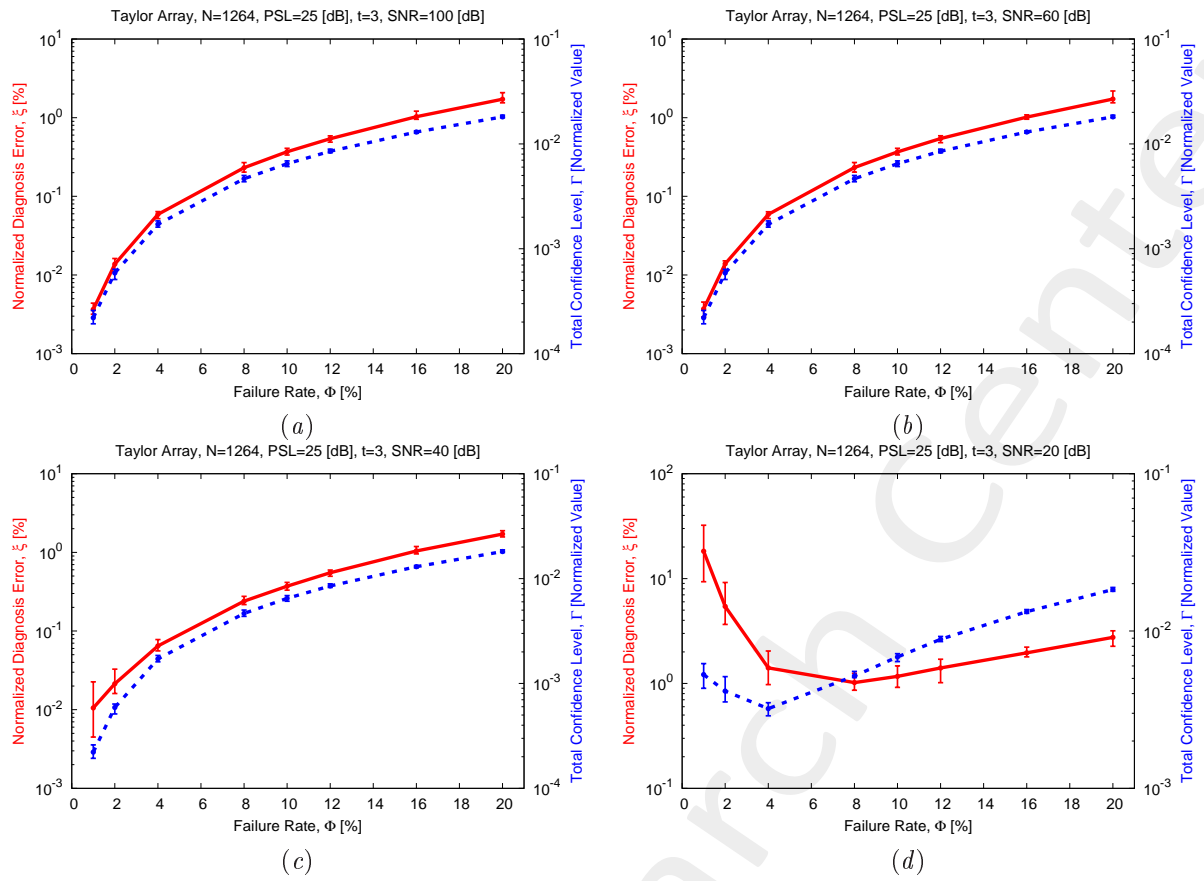


Figure 16: Taylor Array ( $N = 1264$ ,  $PSL = 25$  [dB],  $t = 3$ ) - Behavior of the average, minimum and maximum diagnosis error ( $\xi$ ) and total confidence level ( $\Gamma$ ) versus the failure rate ( $\Phi$ ), for (a)  $SNR = 100$  [dB], (b)  $SNR = 60$  [dB], (c)  $SNR = 40$  [dB], and (d)  $SNR = 20$  [dB].



### 1.3 Taylor Array, $N = 1976$ , Isotropic Sources

#### Parameters

- Gold Array
  - Total number of elements:  $N = 1976$ ;
  - Type of elements: isotropic/ideal<sup>3</sup>;
  - Spacing along  $x$  and  $y$ :  $d_x = d_y = 0.5 [\lambda]$ ;
  - Excitation tapering: Taylor;
    - \* Radius:  $R = 12.5 [\lambda]$ ;
    - \* Transition index:  $t = 3$ ;
    - \* Peak sidelobe level:  $PSL = 25$  [dB];

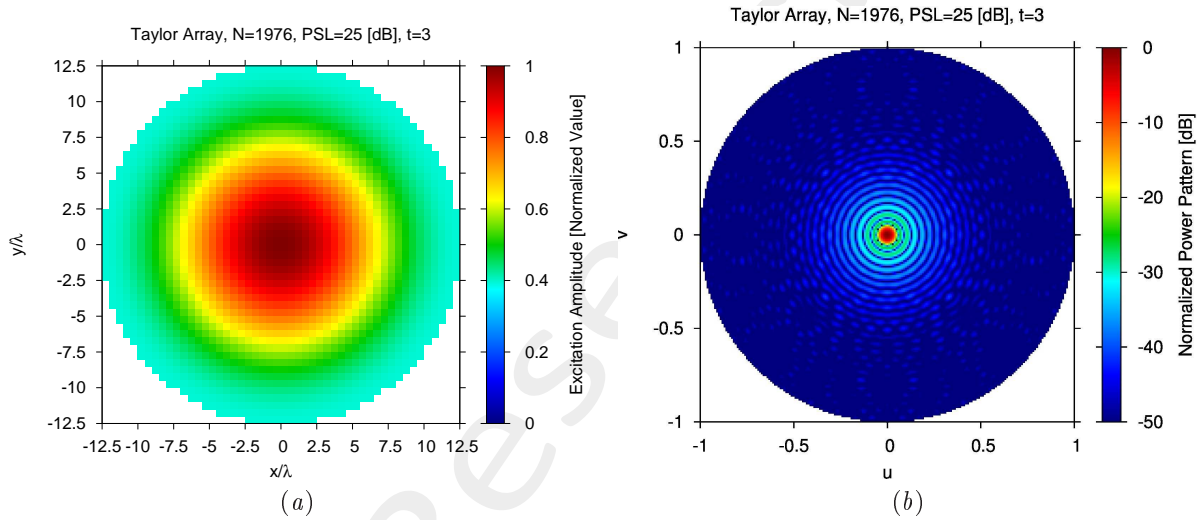


Figure 17: (a) Array excitations and (b) normalized power pattern of the expected array (gold antenna).

- Failed Array
  - Failure factor:  $\kappa = 0$ ;
  - Failure rate: see table below;

$N_f$	$\Phi = \frac{N_f}{N}$
20	1%
40	2%
79	4%
158	8%
316	16%

Table 3: Number of failures ( $N_f$ ) and corresponding failure rate ( $\Phi = \frac{N_f}{N}$ ).

<sup>3</sup>In order to model *isotropic* radiators, let us assume that the embedded elements patterns are equal to  $F_\theta^{(n)}(u, v) = 1$  and  $F_\varphi^{(n)}(u, v) = 0$ , for  $n = 1, \dots, N$ .

- Measurement set-up
  - Type of sampling: uniform sampling in the  $(u, v)$  plane;
  - Number of points in the visible range:  $K = 1961$ ;
  - Ratio between measurements and number of elements:  $\nu = \frac{K}{N} \simeq 1.0$  ( $\nu^{(opt)}$ );
- *BCS* solver
  - Noise variance:  $\eta = 5 \times 10^{-1}$  ( $\eta^{(opt)}$ );
  - Tolerance factor:  $\iota = 10^{-8}$ ;
- Signal-to-Noise-Ratio:  $SNR = \{10; 20; \dots; 100\}$ .

## Results

$\Phi = \frac{N_f}{N} = 1\%$  ( $N_f = 20$ ) - Best and Worst *BCS* Reconstructions

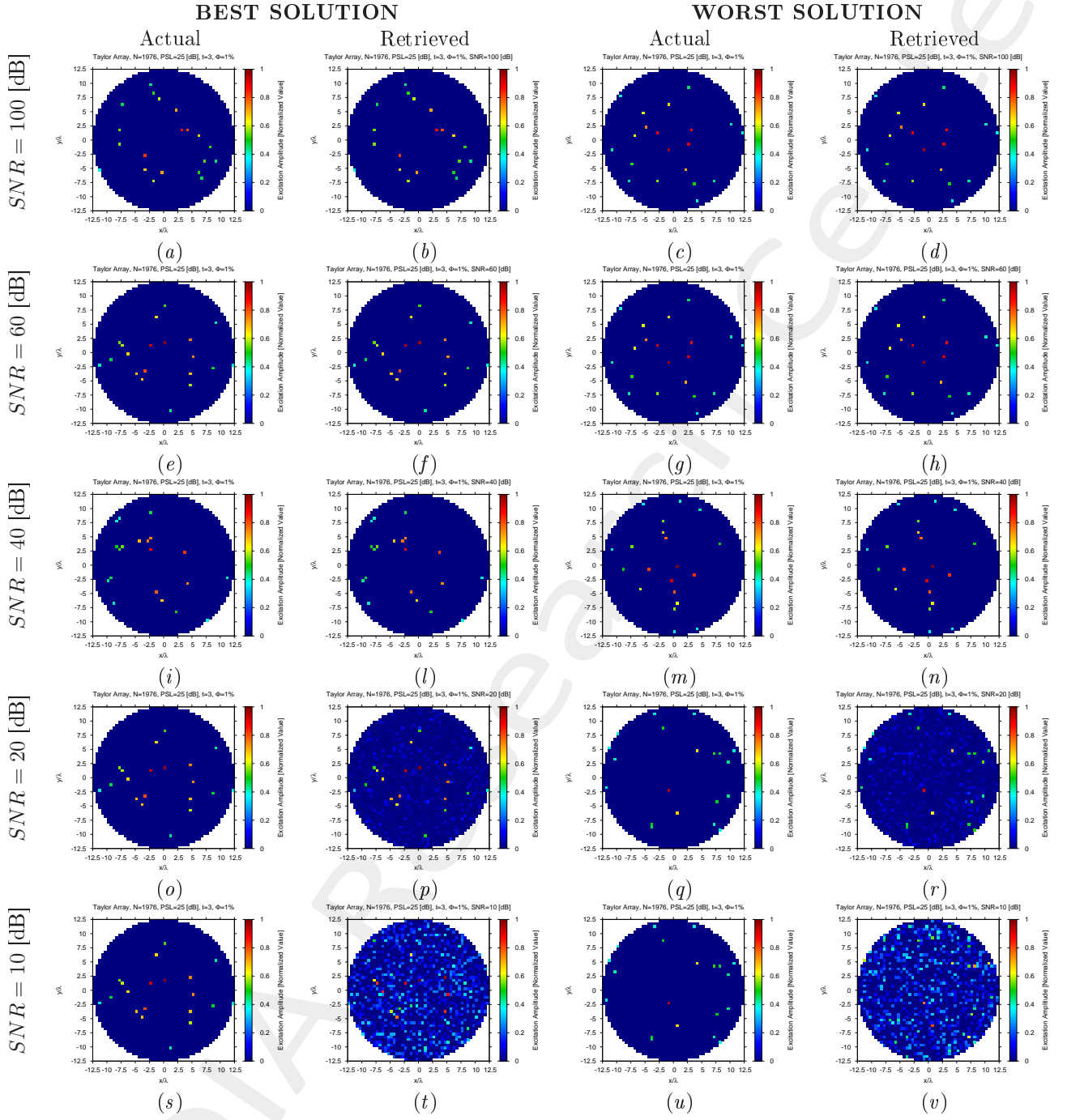


Figure 18: Taylor Array ( $N = 1976$ ,  $PSL = 25$  [dB],  $t = 3$ ,  $\Phi = 1\%$ ) - Best and worst reconstructions by *BCS* under several *SNR* values.

$\Phi = \frac{N_f}{N} = 2\%$  ( $N_f = 40$ ) - Best and Worst *BCS* Reconstructions

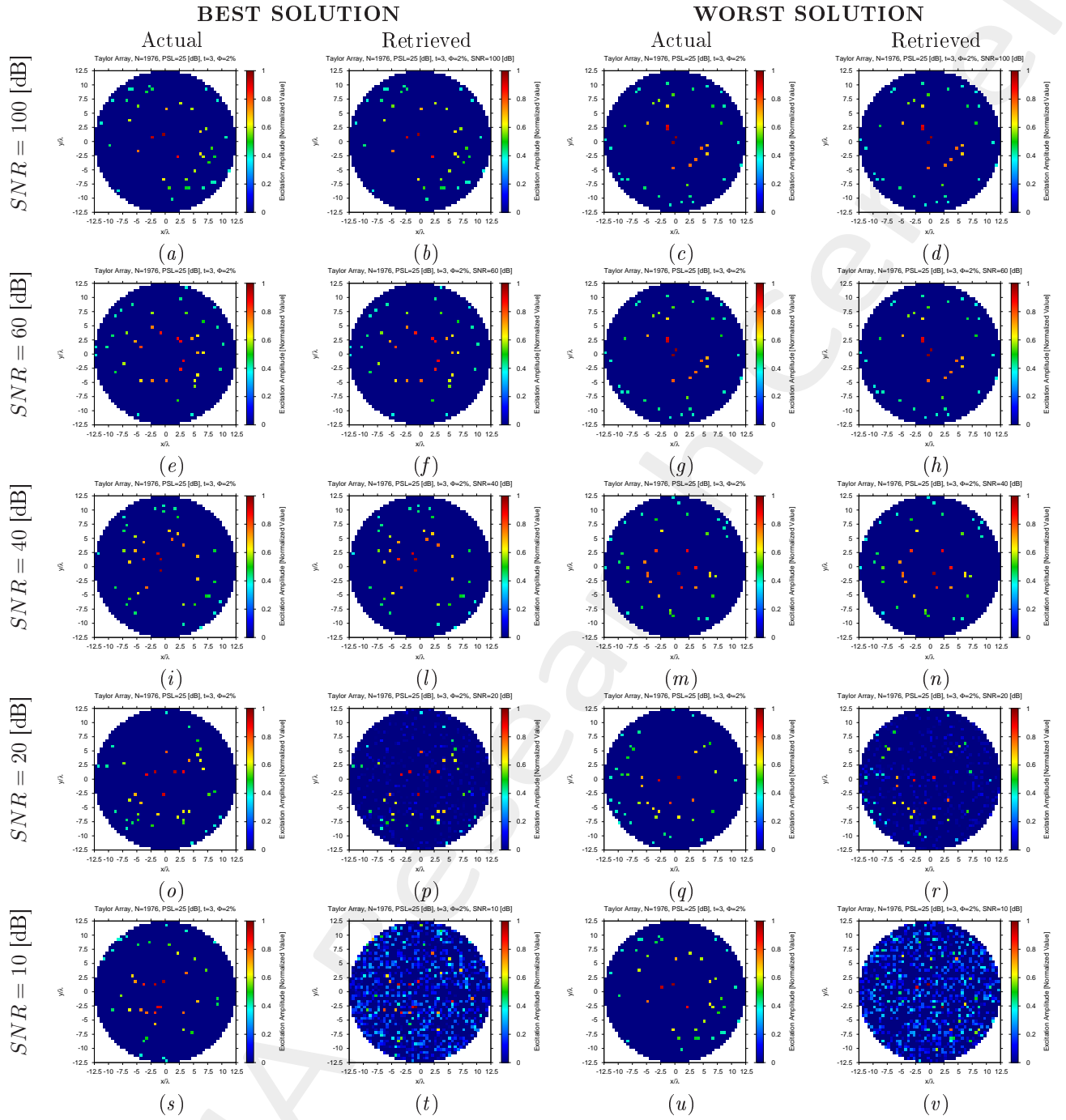


Figure 19: Taylor Array ( $N = 1976$ ,  $PSL = 25$  [dB],  $t = 3$ ,  $\Phi = 2\%$ ) - Best and worst reconstructions by *BCS* under several *SNR* values.

$\Phi = \frac{N_f}{N} = 4\%$  ( $N_f = 79$ ) - Best and Worst *BCS* Reconstructions

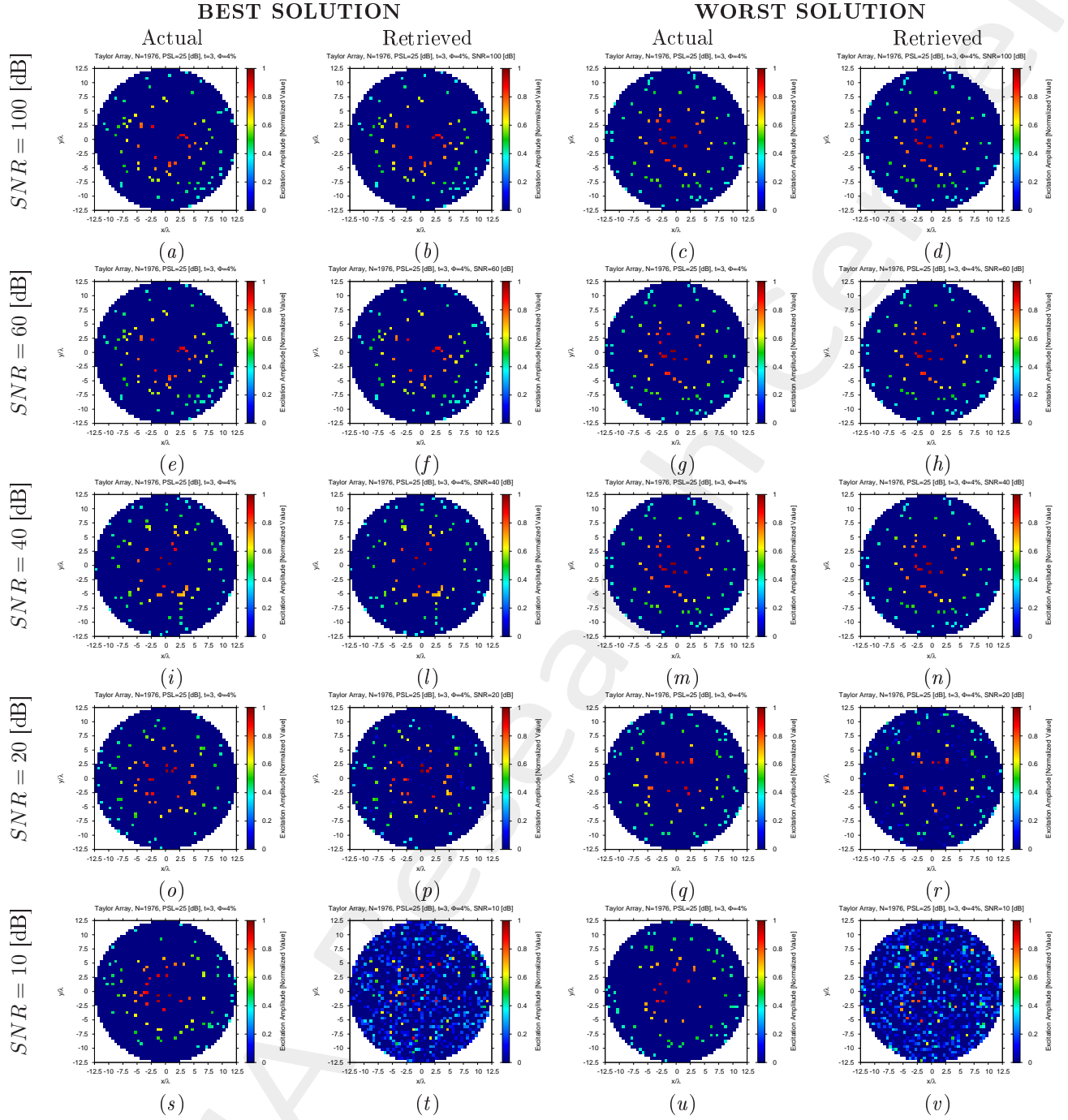


Figure 20: Taylor Array ( $N = 1976$ ,  $PSL = 25$  [dB],  $t = 3$ ,  $\Phi = 4\%$ ) - Best and worst reconstructions by *BCS* under several *SNR* values.

$\Phi = \frac{N_f}{N} = 8\%$  ( $N_f = 158$ ) - Best and Worst  $BCS$  Reconstructions

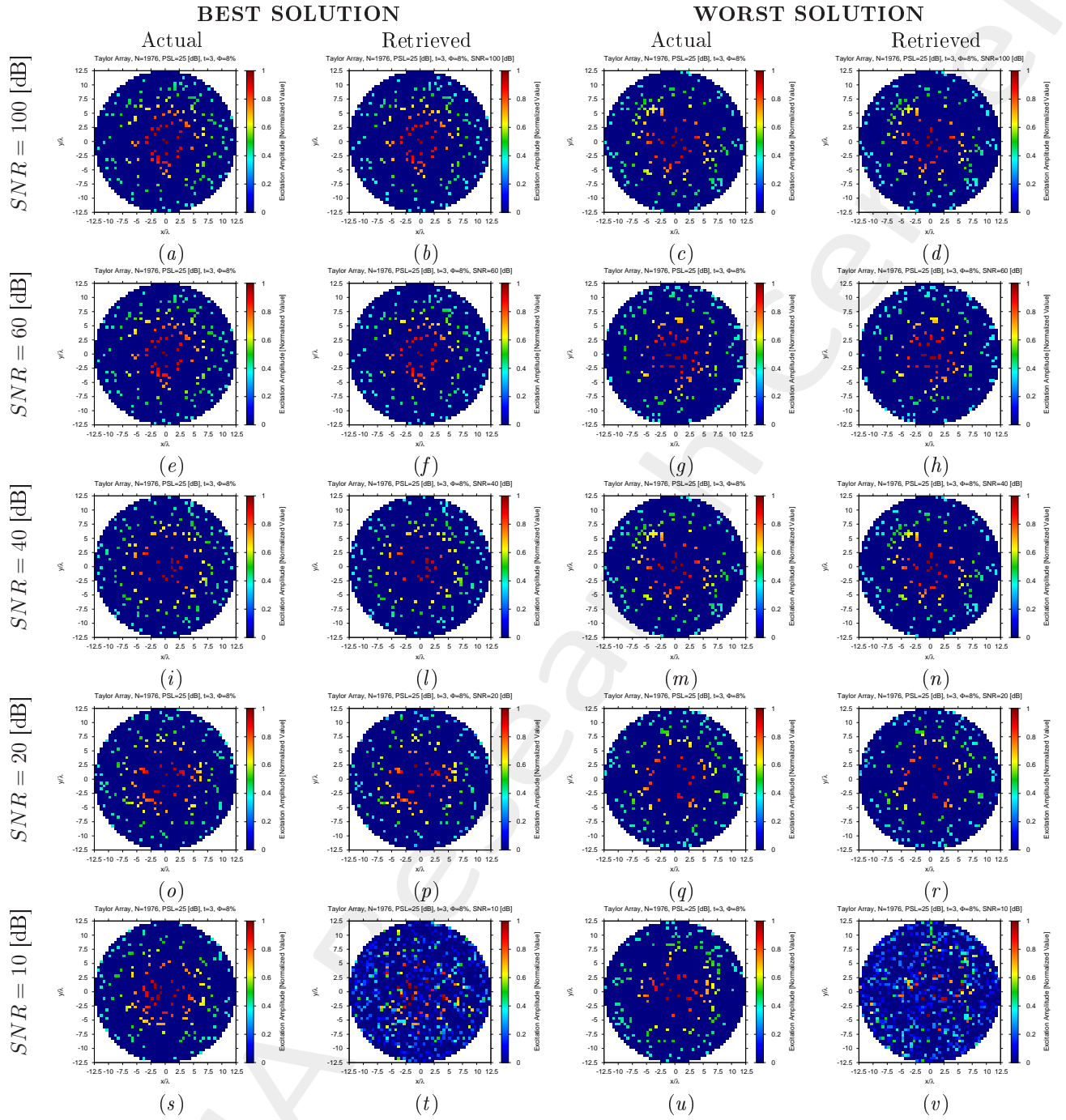


Figure 21: Taylor Array ( $N = 1976$ ,  $PSL = 25$  [dB],  $t = 3$ ,  $\Phi = 8\%$ ) - Best and worst reconstructions by  $BCS$  under several  $SNR$  values.

$\Phi = \frac{N_f}{N} = 16\%$  ( $N_f = 316$ ) - Best and Worst *BCS* Reconstructions

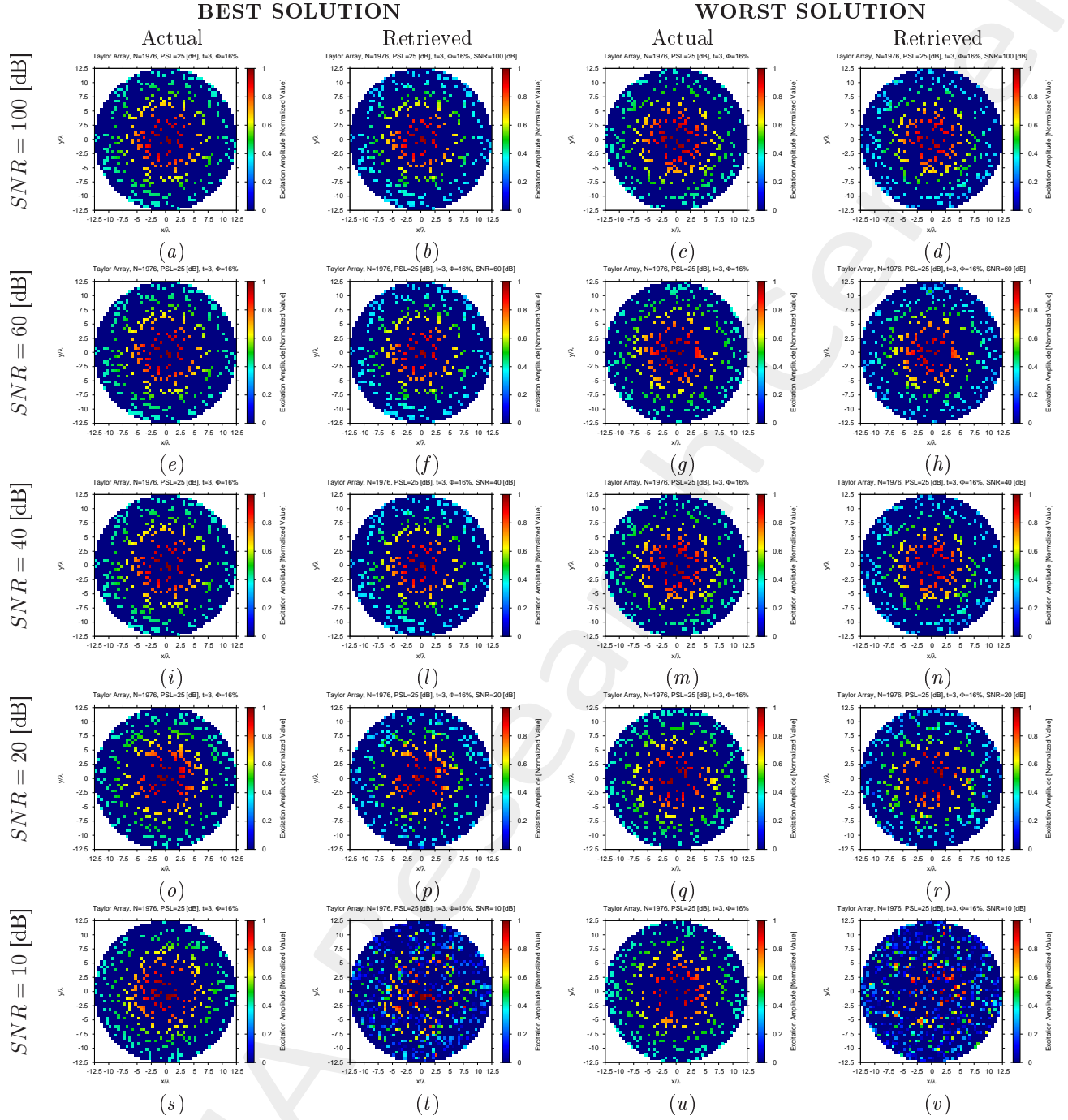


Figure 22: Taylor Array ( $N = 1976$ ,  $PSL = 25$  [dB],  $t = 3$ ,  $\Phi = 16\%$ ) - Best and worst reconstructions by *BCS* under several *SNR* values.

## Diagnosis Error and Confidence Level

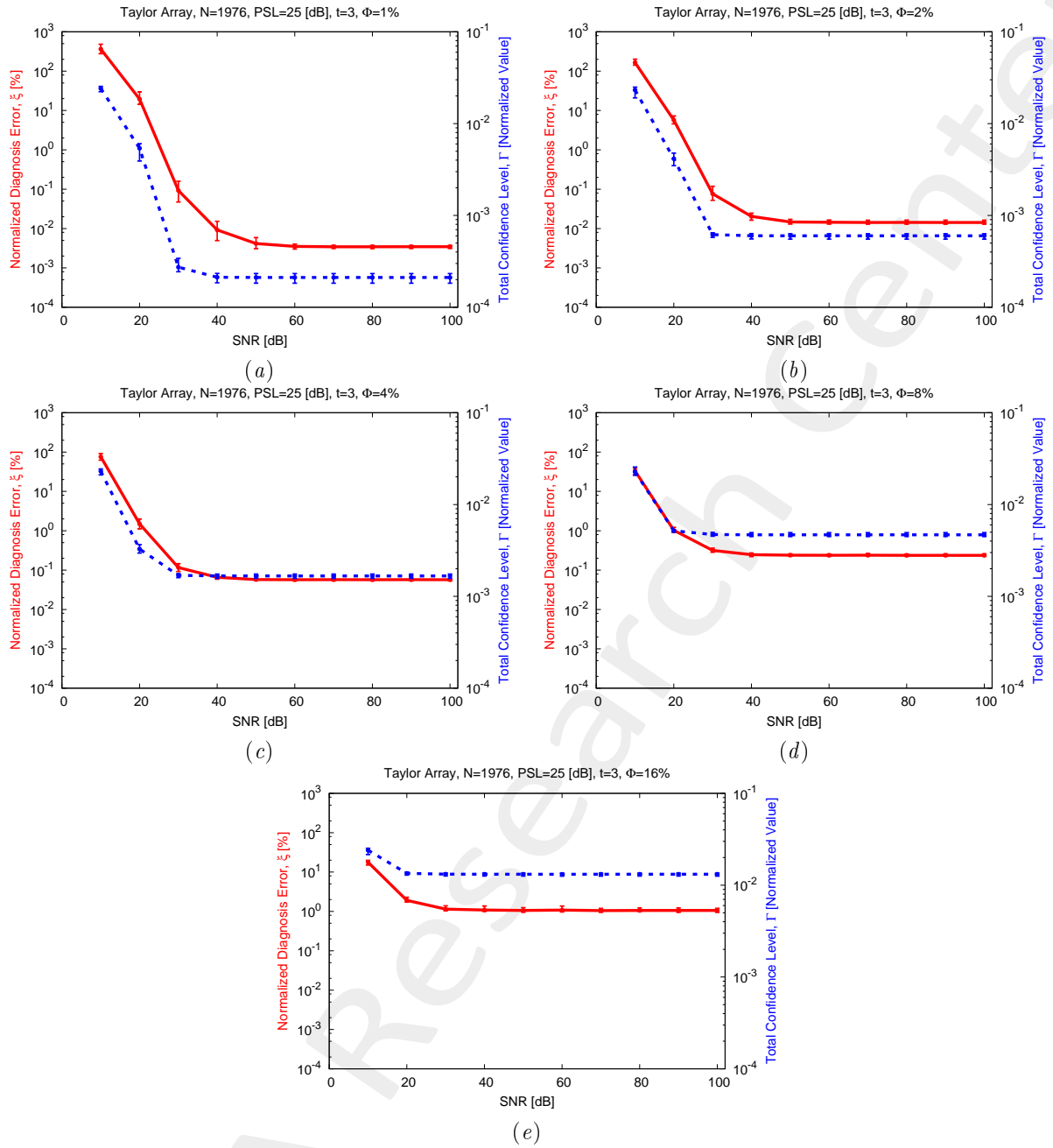


Figure 23: Taylor Array ( $N = 1976$ ,  $PSL = 25$  [dB],  $t = 3$ ) - Behavior of the average, minimum and maximum diagnosis error ( $\xi$ ) and total confidence level ( $\Gamma$ ) versus the  $SNR$ , for (a)  $\Phi = 1\%$ , (b)  $\Phi = 2\%$ , (c)  $\Phi = 4\%$ , (d)  $\Phi = 8\%$ , and (e)  $\Phi = 16\%$ .



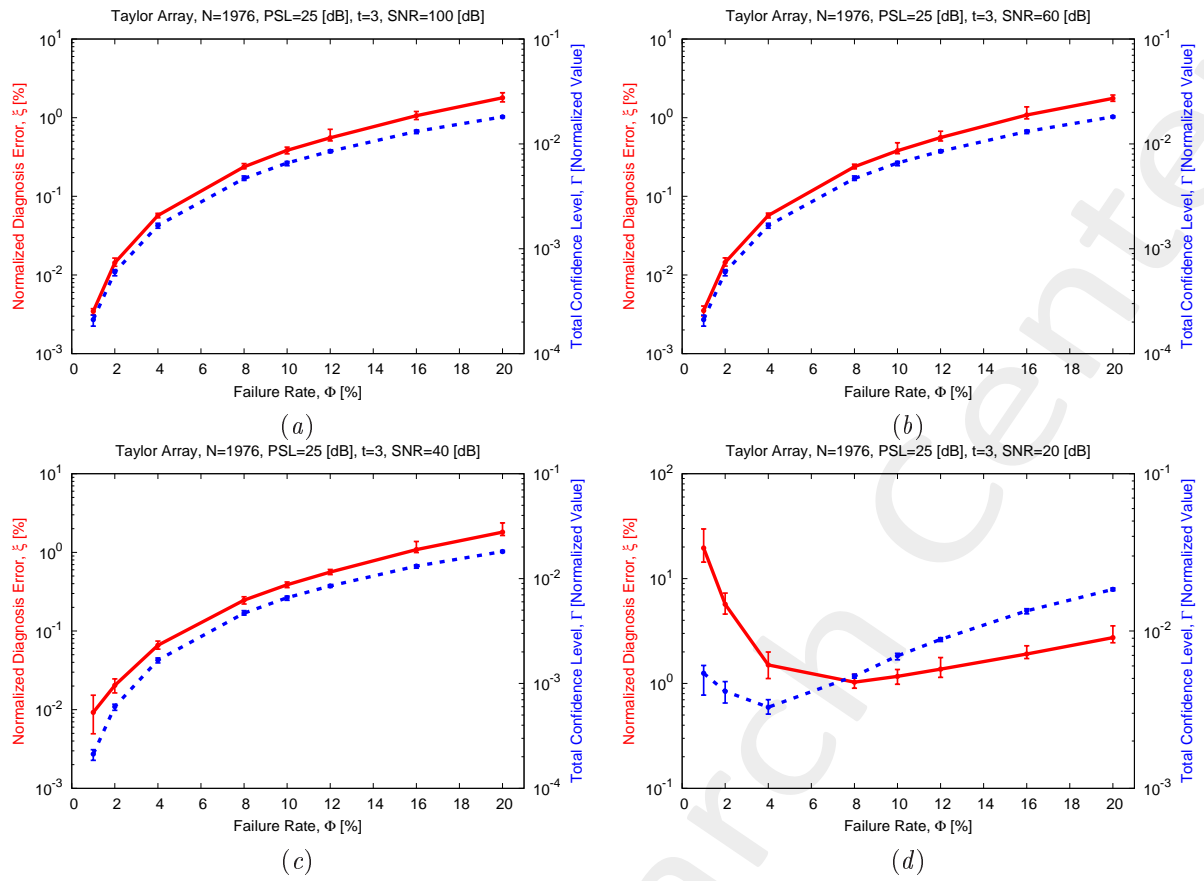


Figure 24: Taylor Array ( $N = 1976$ ,  $PSL = 25$  [dB],  $t = 3$ ) - Behavior of the average, minimum and maximum diagnosis error ( $\xi$ ) and total confidence level ( $\Gamma$ ) versus the failure rate ( $\Phi$ ), for (a)  $SNR = 100$  [dB], (b)  $SNR = 60$  [dB], (c)  $SNR = 40$  [dB], and (d)  $SNR = 20$  [dB].

## 1.4 Taylor Array, Analysis vs. Array Size ( $N$ )

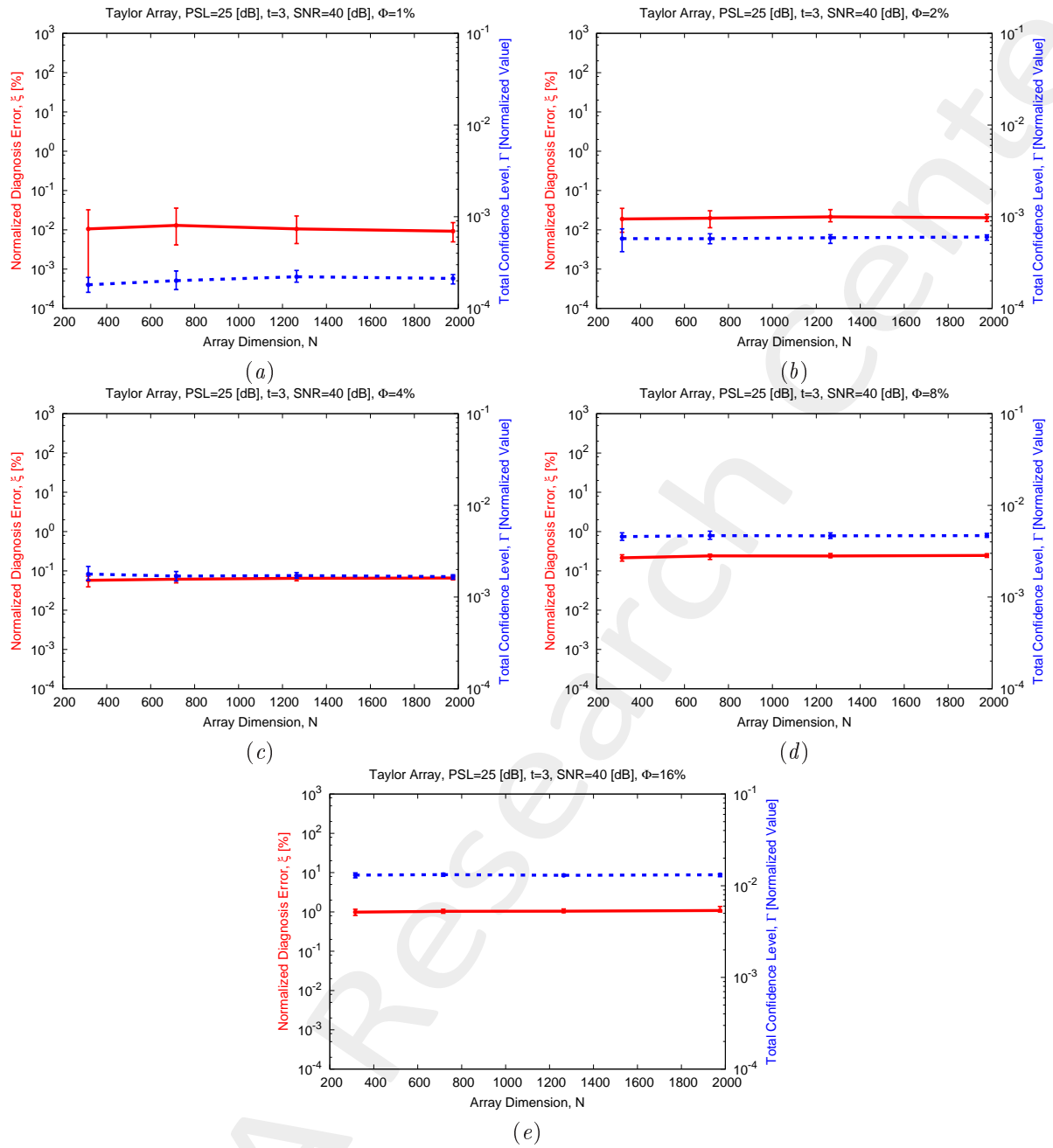


Figure 25: Taylor Array ( $PSL = 25$  [dB],  $t = 3$ ),  $SNR = 40$  [dB] - Behavior of the average, minimum and maximum diagnosis error ( $\xi$ ) and total confidence level ( $\Gamma$ ) versus the array dimension ( $N$ ), for (a)  $\Phi = 1\%$ , (b)  $\Phi = 2\%$ , (c)  $\Phi = 4\%$ , (d)  $\Phi = 8\%$ , and (e)  $\Phi = 16\%$ .

## References

- [1] P. Rocca, G. Oliveri, R. J. Mailloux, and A. Massa, "Unconventional phased array architectures and design methodologies - A Review," *Proc. IEEE*, vol. 104, no. 3, pp. 544-560, Mar. 2016.
- [2] G. Oliveri, G. Gottardi, F. Robol, A. Polo, L. Poli, M. Salucci, M. Chuan, C. Massagrande, P. Vinetti, M. Mattivi, R. Lombardi, and A. Massa, "Co-design of unconventional array architectures and antenna elements for 5G base stations," *IEEE Trans. Antennas Propag.*, vol. 65, no. 12, pp. 6752-6767, Dec. 2017.
- [3] G. Oliveri, P. Rocca, and A. Massa, "Reliable diagnosis of large linear arrays - a Bayesian compressive sensing approach," *IEEE Trans. Antennas Propag.*, vol. 60, no. 10, pp. 4627-4636, Oct. 2012.
- [4] M. Salucci, A. Gelmini, G. Oliveri, and A. Massa, "Planar arrays diagnosis by means of an advanced Bayesian compressive processing," *IEEE Trans. Antennas Propag.*, vol. 66, no. 11, pp. 5892-5906, Nov. 2018.
- [5] A. Massa, P. Rocca, and G. Oliveri, "Compressive sensing in electromagnetics - A review," *IEEE Antennas Propag. Mag.*, pp. 224-238, vol. 57, no. 1, Feb. 2015.
- [6] G. Oliveri, M. Salucci, N. Anselmi, and A. Massa, "Compressive sensing as applied to inverse problems for imaging: theory, applications, current trends, and open challenges," *IEEE Antennas Propag. Mag.*, vol. 59, no. 5, pp. 34-46, Oct. 2017.
- [7] P. Rocca, M. A. Hannan, M. Salucci, and A. Massa, "Single-snapshot DoA estimation in array antennas with mutual coupling through a multi-scaling Bayesian compressive sensing strategy," *IEEE Trans. Antennas Propag.*, vol. 65, no. 6, pp. 3203-3213, Jun. 2017.
- [8] M. Carlin, P. Rocca, G. Oliveri, F. Viani, and A. Massa, "Directions-of-arrival estimation through Bayesian Compressive Sensing strategies," *IEEE Trans. Antennas Propag.*, vol. 61, no. 7, pp. 3828-3838, Jul. 2013.
- [9] L. Poli, G. Oliveri, P. Rocca, M. Salucci, and A. Massa, "Long-distance WPT unconventional arrays synthesis," *J. Electromagn. Waves Appl.*, vol. 31, no. 14, pp. 1399-1420, Jul. 2017.
- [10] G. Oliveri, M. Salucci, and A. Massa, "Synthesis of modular contiguously clustered linear arrays through a sparseness-regularized solver," *IEEE Trans. Antennas Propag.*, vol. 64, no. 10, pp. 4277-4287, Oct. 2016.
- [11] G. Oliveri and A. Massa, "Bayesian compressive sampling for pattern synthesis with maximally sparse non-uniform linear arrays," *IEEE Trans. Antennas Propag.*, vol. 59, no. 2, pp. 467-481, Feb. 2011.
- [12] N. Anselmi, G. Oliveri, M. A. Hannan, M. Salucci, and A. Massa, "Color compressive sensing imaging of arbitrary-shaped scatterers," *IEEE Trans. Microw. Theory Techn.*, vol. 65, no. 6, pp. 1986-1999, Jun. 2017.
- [13] N. Anselmi, G. Oliveri, M. Salucci, and A. Massa, "Wavelet-based compressive imaging of sparse targets," *IEEE Trans. Antennas Propag.*, vol. 63, no. 11, pp. 4889-4900, Nov. 2015.

- [14] L. Poli, G. Oliveri, F. Viani, and A. Massa, "MT-BCS-based microwave imaging approach through minimum-norm current expansion," *IEEE Trans. Antennas Propag.*, vol. 61, no. 9, pp. 4722-4732, Sep. 2013.
- [15] G. Oliveri, N. Anselmi, and A. Massa, "Compressive sensing imaging of non-sparse 2D scatterers by a total-variation approach within the Born approximation," *IEEE Trans. Antennas Propag.*, vol. 62, no. 10, pp. 5157-5170, Oct. 2014.
- [16] L. Poli, G. Oliveri, and A. Massa, "Imaging sparse metallic cylinders through a local shape function bayesian compressive sensing approach," *J. Opt. Soc. Am. A*, vol. 30, no. 6, pp. 1261-1272, 2013.
- [17] L. Poli, G. Oliveri, P. Rocca, and A. Massa, "Bayesian compressive sensing approaches for the reconstruction of two-dimensional sparse scatterers under TE illumination," *IEEE Trans. Geosci. Remote Sens.*, vol. 51, no. 5, pp. 2920-2936, May 2013.
- [18] L. Poli, G. Oliveri, and A. Massa, "Microwave imaging within the first-order Born approximation by means of the contrast-field Bayesian compressive sensing," *IEEE Trans. Antennas Propag.*, vol. 60, no. 6, pp. 2865-2879, Jun. 2012.
- [19] G. Oliveri, L. Poli, P. Rocca, and A. Massa, "Bayesian compressive optical imaging within the Rytov approximation," *Opt. Lett.*, vol. 37, no. 10, pp. 1760-1762, 2012.
- [20] G. Oliveri, P. Rocca, and A. Massa, "A Bayesian compressive sampling-based inversion for imaging sparse scatterers," *IEEE Trans. Geosci. Remote Sens.*, vol. 49, no. 10, pp. 3993-4006, Oct. 2011.
- [21] N. Anselmi, L. Poli, G. Oliveri, and A. Massa, "Iterative multi-resolution bayesian CS for microwave imaging," *IEEE Trans. Antennas Propag.*, vol. 66, no. 7, pp. 3665-3677, Jul. 2018.
- [22] L. Poli, P. Rocca, G. Oliveri, and A. Massa, "Failure correction in time-modulated linear arrays," *IET Radar, Sonar & Navigation*, vol. 8, no. 3, pp. 195-201, 2014.